Mohammad Fikry* and Alhussein M. Al-Awaadh

Characteristics of Dynamics Sorption Isotherms of Date Flesh Powder Rich in Fiber

DOI 10.1515/ijfe-2015-0223

Abstract: Dynamic vapor sorption equipment (AQUADVS) was used to determine adsorption and desorption isotherms for powder rich in fiber (PRF) produced from Palm Date flesh of Sifri cultivar (*Phoenix dactylifera* L.) at temperatures 25, 35 and 45 °C in a wide range of water activity (0.09–0.87). Equilibrium was achieved within 29 and 25 h for the adsorption and desorption process respectively. The obtained data were fitted to ten models (Peleg, GAB, BET, Halsey, Oswin, Smith, Modified Henderson, Adam and Shove, Modified Oswin and Modified Halsey). The results indicated that the PRF followed type III behavior. The empirical Peleg model was found to be the best to represent the experimental data in the water activity range 0.09–0.87. The isosteric heat of sorption and the differential entropy decreased by increasing the moisture content and can be predicted by polynomial functions. Glass transition temperatures (T_g) of PRF were determined. The T_g decreased as the moisture content increased and can be correlated using the Gordon and Taylor model ($R^2 = 0.976$). The PRF should be stored at moisture less than 9 d.b.% and temperature less than 35 °C.

Keywords: dynamic sorption isotherms, isosteric heat of sorption, differential entropy, Date powder, glass transition

1 Introduction

Palm Dates (*Phoenix dactylifera* L.) is a very popular fruit throughout the Middle East and North Africa countries. Large quantities of Palm Dates products, such as date juice concentrates (spread, syrup and liquid sugar), date-honey, date-jam, date-vinegar, and date pastes, are produced. During the peak of the harvesting season, considerable quantities of the fruit are wasted. In addition, wastes are generated from transformative processes of Dates. These by-products are generally discarded and eventually constitute environmental problem or sometimes are used as animal feed. This constitutes a real economic loss since some of these by-products can be converted to high added value products such as powder rich in fibers (PRF). In fact, it was possible to produce fine PRF from Palm Date flesh (Sifri cultivar) with total dietary fiber 72.65 %, water holding capacity 6.03 g water/g dry sample and oil holding capacity 9.1 g oil/g dry sample [1]. Thus, further investigation of sorption isotherm of this promising PRF is important.

Usually, powders are hygroscopic material which can absorb moisture from the surrounding environment easily. Thus, moisture sorption isotherms are considered a useful tool to understand the moisture relationship of a powder and consequently its stability problems [2]. The relationship between the equilibrium moisture content and water activity of the food, over a range of values, at a constant temperature and under equilibrium conditions, gives a moisture sorption isotherm when expressed graphically. This isotherm curve consists of two different paths; adsorption or desorption. The sorption processes are not fully reversible, therefore a distinction can be made between the isotherms by determining whether the moisture levels within the product are increasing or decreasing [3].

The quality of preserved foods depends on the moisture content, moisture migration, and moisture uptake by the food material during storage. The equilibrium moisture content can be defined as the point when the vapor pressure of water present in the food equals that of its surroundings [4].

Many methods are available for determining water sorption isotherms, of which, gravimetric method. The gravimetric method includes the measurement of weight changes, which can be determined both continuously and discontinuously in dynamic or static systems (i. e. air may be circulated or stagnant). Continuous methods employ the use of electro-balances or quartz spring balances. In the discontinuous systems, salt or sulfuric acid solutions are placed in vacuum or atmospheric systems with the food material, to give a measure of the equilibrium relative humidity (ERH) [3].

***Corresponding author: Mohammad Fikry,** Department of Agricultural Engineering, King Saud University, P.O. Box 2460, Riyadh 11451, Saudi Arabia, E-mail: moh.fikry@live.com
Alhussein M. Al-Awaadh, Department of Agricultural Engineering, King Saud University, P.O. Box 2460, Riyadh 11451, Saudi Arabia, E-mail: assiry@ksu.edu.sa

Dynamic vapor sorption (DVS) method could overcome the disadvantages encountered with the discontinuous system (slowness of the equilibrium process, the possibility of mold or bacterial growth on samples at high relative humidity (RH) and difficulty). The DVS system requires a mixture of dry nitrogen and saturated water vapor instead of the use of saturated salt solutions in order to provide the desired RH. In this case, the equilibration is more rapid due to the small sample chamber and the continuous flow of dry nitrogen. Such system avoids the risk of microorganisms growth at high RH and therefore enables the measurement of the same sample for absorption and desorption isotherms [5]. Several researchers used DVS to investigate the behavior of sorption isotherms of some products such as Garlic powder [6], Wheat flour components [7], sodium starch glycolates [8] and pharmaceutical granules [9].

Moisture desorption–adsorption isotherms and mathematical models to describe sorption isotherms of various products have been studied by several researchers. Some researchers observed that the isotherm curves exhibited type II for some materials such as starch [3], rice grain [5] and Blackberry pulp powder [10]. Other products exhibited type III isotherm curves such as Apple and Mango slices [11], Firm ripe plantain [12], berry powders (strawberries, blueberries, raspberries, and blackberries) [13] and Pineapple slices [14]. It should be noticed that type III found with products high in sugar contents.

Regardless of types of the sorption isotherm curves, several models can be used to model the adsorption isotherm. It has been reported that the modified Oswin equation was the best fit to describe the adsorption isotherms of both leaves and stems of lemon balm using an automatic, gravimetric analyzer (DVS system) [15]. Peleg equation gave the most adequate model to describe sorption behavior of different varieties of rice at 25 °C over a water activity range of 0.09–0.98 [5]. The GAB equation described appropriately the experimental data for pineapple pulp powder over a wide range of a_w at 20, 30, 40, and 50 °C [16]. The GAB isotherm model was found to be appropriate for describing the experimental data of blackberry pulp powders [10]. Sorption data of peel and leaves of orange were best fitted by the Peleg model at 40, 50 and 60 °C in a wide range of water activity (0.109–0.891) [17]. Sorption data were best fitted by the Peleg model at water activities and temperatures ranging from 0.058 to 0.898 and from 30 to 50 °C, respectively for Tunisian olive leaves [18]. The Halsey equation and GAB gave the best fit to the experimental sorption data for grapes, apricots, apples and potatoes at 30, 45, and 60 °C using the static-gravimetric method [19]. The Peleg model was the best model to describe the experimental data of starch powder at water activities ranging from 0.05 to 0.95 and temperatures 30, 45 and 60 °C using a gravimetric technique [3]. Experimental sorption data for lemon peel were best fitted by the GAB model at four different temperatures (20, 30, 40 and 50 °C) and wide ranges of moisture content (5.381–0.002 kg water/kg dry solid) and water activity (0.984–0.106) [20]. The GAB and modified BET models were found to be the most suitable to model the sorption data of *Citrus* leaves at 30, 40 and 50 °C with water activity ranging from 5 % to 90 % [21]. The best fit was obtained with BET and GAB models for Sicilian lemon residues [22].

The net isosteric heat (q_{st}) is defined as the total heat of sorption in the material minus the latent heat of vaporization of water, at constant temperature [23]. The heat of adsorption is a measure of the energy released on sorption, and the heat of desorption is the energy requirement to break the intermolecular forces between the molecules of water vapor and the surface of adsorbent [24]. Thus, the heat of sorption is considered as indicative of the intermolecular attractive forces between the sorption sites and water vapor [25]. The isosteric heat of sorption was computed from the sorption data by applying the Clausius–Clapeyron equation for starch powders [26], *Citrus reticulate* leaves [21], Tunisian olive leaves [18], orange (*Citrus sinensis*) peel and leaves [17], leaves and stems of lemon balm [15], tow mints [27], withered leaves, black and green tea [28], grapes, apricots, apples and potatoes [19] and *Chenopodium ambrosioides* leaves [29]. Their results indicate an increase in the heat of sorption with decreasing moisture content.

The differential entropy (ΔS) of a material is proportional to the number of available sorption sites at a specific energy level [30]. It decreased with increasing moisture content. The strong dependence of differential entropy on moisture content with an exponential trend was found for starch powders [26]. It can be characterized by a power law equation for tow mints [27].

Since sorption isotherm is essential for evaluation of storage stability, the glass transition temperature is an important factor to be considered. Where the glass transition temperature (T_g) is defined as the temperature at which a solid "glass" system is transformed to the rubbery state "liquid-like". In glassy state, molecular mobility is extremely slow, due to the high viscosity of the matrix (about 10^{12} Pa.s). Thus the T_g can be taken as a reference parameter to characterize properties, quality, stability and safety of food materials [31]. Above glass

transition temperature (T_g) structural transformations may occur in amorphous powder such as stickiness, caking and agglomeration. These changes play an important role in the ability to store dried food products [32]. Many researchers studied the plasticization effect of moisture content on T_g of several food products such as spray dried tomato pulp powder [33], freeze-dried pineapple powder [34], freeze-dried onion powder [35], Kiwi fruit [36] and papaya [37].

Knowledge of the moisture sorption characteristics and glass transition temperature of a PRF is important for predicting its stability through storage period and selecting adequate packaging materials.

For the best knowledge of the authors, no published work related to moisture sorption and glass transition temperature of PRF produced from Date flesh was found. Thus the objectives of this work were to provide trustworthy experimental data for the sorption characteristics of PRF, model the sorption isotherms, determine the isosteric sorption heat and the entropy of sorption and define the glass transition temperature and moisture content relationship.

2 Materials and methods

2.1 Sample preparation

The Dates fruits (Sifri cultivar) were obtained from a local Date market (Riyadh, Saudi Arabia). It was processed to obtain date PRF, details of the preparation can be found in reference [1]. Where the soluble solids from Date flesh were extracted using hot water at 70 ± 2 °C for 15 min. Cycles of extractions were used starting with 1:2.5 (w/w) Date: water ratio through a plate filtration unit. Then the suspension was filtered using filtration plates at pressure equal to three bars. Cycles of extraction with water were repeated till the total dissolved solids (TSS) approached 1% or less in the filtrate. Samples of filtration cake obtained from the filtration unit were dried in a lab scale convective dryer at 50 ± 1.5 °C and air velocity 2 ± 0.5 m/s till moisture content was less than 9% [38]. The dried samples were grinded to fine size (125–180 μm). Then, the PRFs were stored in very well sealed glass containers at 4 °C until analysis.

2.2 Sorption isotherms measurements

The sorption isotherms of the samples were obtained by dynamic vapor sorption instrument (DVS) (AQUADVS, Quantachrome Instruments, Florida, USA, 2009). The instrument consists of an electronic microbalance with two sample pans made of quartz and a humidifier in a chamber with temperature controller. A mixture of dry nitrogen and saturated water vapor flows over the pans. The relative humidity of the mixture was regulated by two electronic mass flow controllers. The equipment was connected to a computer, allowing pre-programming of stepwise variation of relative humidity at set temperature and continuous measurement of temperature, humidity and mass during the sorption process.

Pre-dried samples of PRF with weight of 90 ± 1.6 mg and initial moisture content (X_w) of 7.87 ± 0.61% d.b. were used for the different experiments. The sorption isotherms were obtained at temperatures of 25, 35 and 45 °C. The relative humidity was changed from 10 to 90% at a constant temperature. For each experiment, sample was placed into the pan of the equipment. Each sample was first dried (purge step) by passing dry nitrogen until a constant weight of the sample was reached. Subsequently, the relative humidity was increased stepwise until the sample weight was equilibrated at each relative humidity step. Weight, temperature and relative humidity data were recorded in 5 min time intervals. The software was programmed so that the equilibrium was reached when the change in sample mass as a function of time was lower than 0.005%/min. The above criteria were met for all of the experiments. All of the experiments were done in triplicate. To get the sorption isotherms, the moisture content (X_w) of the sample, expressed in kg water per kg dry solids, was computed at equilibrium of each relative humidity step.

2.3 Measurement of glass transition temperature

Equilibrated PRF samples of 10 mg were taken for differential scanning calorimetry (DSC) analysis. The glass transition temperature was determined by DSC (DSC 6000, PerkinElmer, USA). The samples were heated at 10 °C/min between −60 °C and 100 °C in an inert atmosphere. The reference was an empty pan, while liquid nitrogen was used for sample cooling before the runs. The midpoint of the glass transition was considered as the characteristic temperature of the transition. The moisture contents of the samples were determined using Halogen moisture analyzer (HR73, METELLER TOLEDO, Switzerland).

2.4 Data analysis

2.4.1 Modeling of sorption isotherms

Ten mathematical equations were used to fit the adsorption and desorption isotherms data of PRF at the different temperatures as shown in Table 1. The models are presented in terms of equilibrium moisture content, X_e dry basis (kg/kg d.b.), water activity a_w, temperature T (°C) and model constants. To evaluate the ability of each model to fit the experimental sorption data, results were expressed as mean values (standard deviation) of the three separate determinations. The selected mathematical models were evaluated using the statistical parameters, namely, coefficient of determination (R^2), the mean relative percent error (P_e), the standard error of estimate (SSE) and root mean square error (RMSE). These four different criteria were evaluated by MATLAB R2010a [39].

2.4.2 Determination of isosteric heat of sorption and the differential entropy

The net isosteric heat of sorption (q_{st}) was determined by subtraction of the water vaporization heat from the total heat of sorption (Q_{st}). The q_{st} could be determined from experimental data using Clausius–Clapeyron equation [10].

$$\ln(a_w) = -\frac{q_{st}}{RT_k} + \frac{\Delta S}{R} \quad (1)$$

$$Q_{st} = q_{st} + \lambda \quad (2)$$

where the vaporization heat of pure water (λ) (J/mole) was calculated by:

$$\lambda = R[6687 - 5.31^{*}T_k] \quad (3)$$

where R is the ideal gas constant (8.314 J/mole.K); T_k absolute temperature (K) and ΔS is the differential entropy (J/mole.K).

In this study, the isosteric heat of sorption and the differential entropy (ΔS) of adsorption and desorption of water at each moisture content were obtained by fitting eq. (1) to the equilibrium moisture content data. After plotting ln (a_w) versus $1/T_K$ at constant moisture content, the isosteric heat of sorption was determined from the slope which was equal to $-q_{st}/R$ and the ΔS was computed from the linear coefficient ($\Delta S/R$). This procedure was repeated for many values of equilibrium moisture content in order to determine the dependence of q_{st} on the equilibrium moisture content. Although this approach assumes that isosteric heat of sorption does not change with temperature, the application of this method requires sorption data at three temperatures at least [18, 19].

2.4.3 Water plasticization behavior

To predict the plasticization effect of water, glass transition temperature and moisture content data were fitted to the model proposed by Gordon and Taylor [50]:

$$T_g = \frac{(1-X_w)T_{gs} + kX_wT_{gw}}{(1-X_w) + kX_w} \quad (4)$$

Table 1: The models applied to the experimental adsorption and desorption data of Date powder rich in fiber (PRF).

No	Model name	Equations	References
1	Peleg	$X_e = {}_1(a_w)^{C_2} + {}_3(a_w)^{C_4}$	[40]
2	GAB	$X_e = \frac{X_m CKa_w}{(1-Ka_w)(1-Ka_w+CKa_w)}$	[41]
3	BET	$X_e = \frac{X_m ca_w}{[(1-a_w)+(c-1)(1-a_w)a_w]}$	[42]
4	Halsey	$X_e = \left(-\frac{A}{\ln a_w}\right)^{1/B}$	[43]
5	Oswin	$X_e = k(a_w/1-a_w)^n$	[44]
6	Smith	$X_e = A - B(\ln(1-a_w))$	[45]
7	Modified Henderson	$X_e = \{\ln(1-a_w)/[-k(T+c)]\}^{1/n}$	[46]
8	Adam and Shove	$X_e = A + Ba_w + Ca_w{}^2 + Da_w{}^3$	[47]
9	Modified Oswin	$X_e = (A+BT)\left[\frac{a_w}{(1-a_w)}\right]^C$	[48]
10	Modified Halsey	$X_e = \left[-\frac{\exp(A+BT)}{\ln a_w}\right]^C$	[49]

Note: X_e is the equilibrium moisture content (kg/kg dry solid); X_m is the mono-layer moisture content (kg/kg dry solid); A, B, C, C1, C2, C3, C4, D, K and n: model constants (dimensionless).

where T_g, T_{gs} and T_{gw} are the glass transition temperatures of the mixture, solids, and water, respectively, X_w is the mass fraction of water and k is the model constant.

3 Results and discussion

3.1 Moisture sorption profiles

Figure 1 represents the temporal profile of moisture adsorption (a) and desorption (b) of PRF at 25 °C, as an example of using a dynamic vapor sorption instrument. It can be observed that the moisture adsorption increased with increasing relative humidity, while the opposite was noticed in the case of desorption process. It took up to 29 and 25 h to reach equilibrium state for the adsorption and desorption process respectively.

3.2 Experimental results

The experimental results of the adsorption and desorption isotherms of the PRF obtained at different temperatures are presented in Figures 2 and 3, respectively. The adsorption isotherms follow type III shape, which characterizes the products that hold small amounts of water at low water activity levels and large amounts at high relative humidity levels according to the BET classification [51]. Such relationship has been reported for lemon peel [20]. It was observed in Figure 2 that the equilibrium moisture content (X_e), at constant temperature, increased by increasing a_w. The opposite was observed in the case of desorption where the X_e decreased as a_w decreased (Figure 3). This behavior of adsorption and desorption experiments was similar to that reported for many food products, such as Citrus reticulata leaves [21], leaves and stems of lemon balm [15], Tunisian olive leaves [18] and orange peel and leaves [17]. Also, the results revealed that there was no effect of temperature on the sorption isotherms of PRF. Kaya and Kahyaoglu [52] found similar result for tarragon leaves. That could be due to the small temperature range studied in the present work which was not enough to cause an increase in the excitation state of water molecules [53].

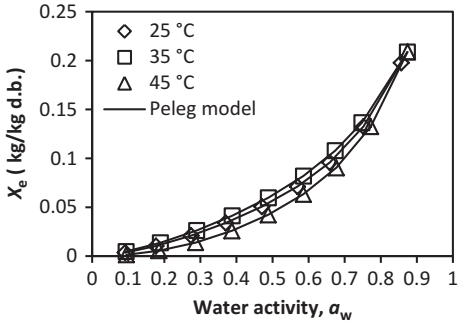

Figure 2: Experimental and predicted adsorption isotherms obtained for PRF at 25, 35 and 45 °C.

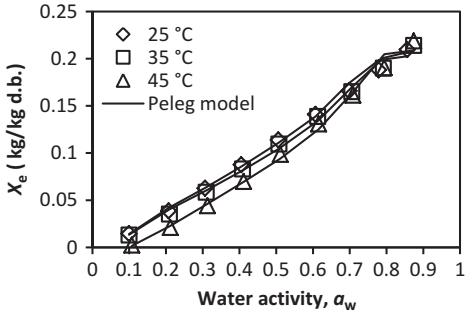

Figure 3: Experimental and predicted desorption isotherms obtained for PRF at 25, 35 and 45 °C.

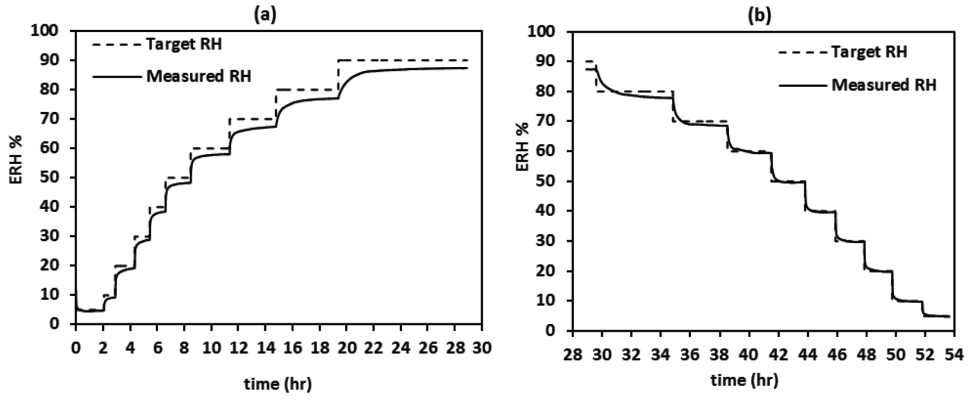

Figure 1: Temporal moisture adsorption (a) and desorption (b) profiles for PRF under stepwise change of equilibrium relative humidity (ERH) at 25 °C.

3.3 Moisture sorption hysteresis

Moisture sorption hysteresis is the phenomena in which two different paths exist between the adsorption and desorption isotherms. The extent of hysteresis is related to the nature and state of the components in a food. It may reflect their structural and conformational rearrangement, which alters the accessibility of energetically favorable polar sites, and thus, may hinder the movement of moisture [54].

The hysteresis loops were seen at the temperatures (25, 35 and 45 °C) as shown in Figures 4, 5 and 6, respectively. This phenomenon has been explained by several researchers, among which, Al Hodali [55] who considered a solid structure pore connected to its surrounding by a small capillary. It has been reported that during adsorption, the capillary begins to fill as a result of the rise in relative humidity, while the pore was still empty. When the partial pressure of vapor in the air becomes higher than the vapor pressure of liquid in the capillary, the moisture will move into the pore. For desorption, the pore was initially full of liquid at saturation. This liquid could escape only when the pressure of the surrounding air becomes lower than the vapor pressure of liquid inside the capillary. As the system of pores has generally a large range of capillary diameters, the differences between adsorption and desorption were observed [21].

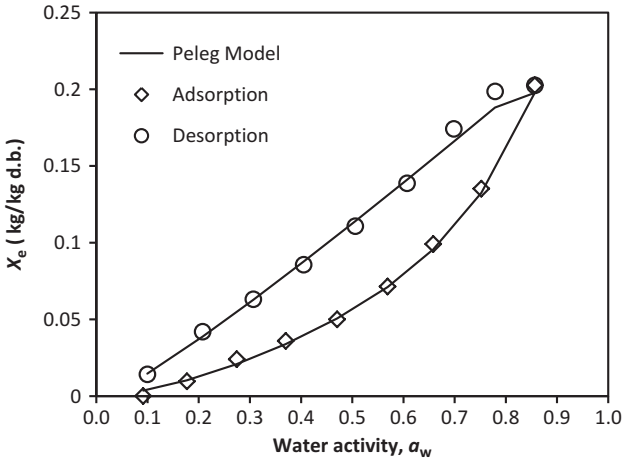

Figure 4: Experimental and predicted sorption data (desorption and adsorption) for the PRF obtained at 25 °C (hysteresis loop).

It was observed that at the same water activity, the equilibrium moisture content was higher for the desorption curve than for the adsorption one as shown in Figures 4, 5 and 6 corresponding to temperatures 25, 35 and 45 °C, respectively. This hysteresis behavior could be due to the pre-drying in which the samples were subjected to during the adsorption process [56]. Such behavior was observed for orange peel and leaves [17].

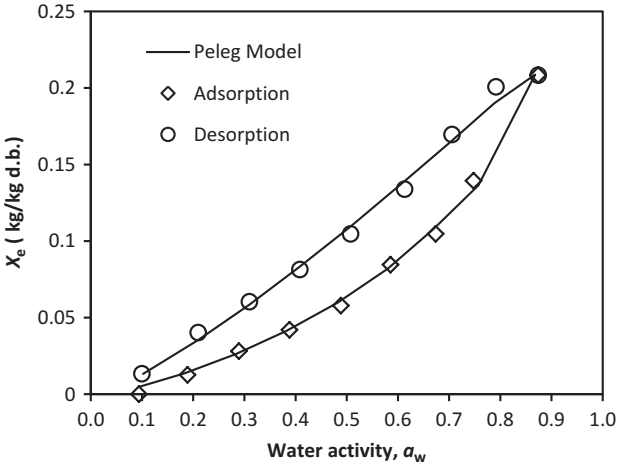

Figure 5: Experimental and predicted sorption data (desorption and adsorption) for the PRF obtained at 35 °C (hysteresis loop).

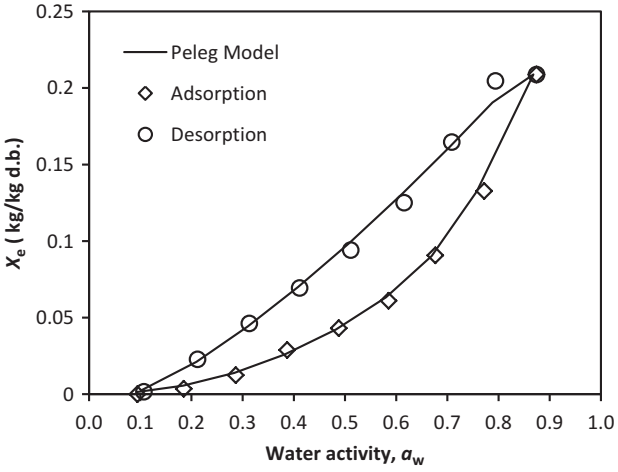

Figure 6: Experimental and predicted sorption data (desorption and adsorption) for the PRF obtained at 45 °C (hysteresis loop).

3.4 Modeling data

The experimental data of the adsorption and desorption curves of PRF were fitted to ten isotherm models as listed in Table 1. The results of non-linear regression analysis of fitting the adsorption and desorption equations to the experimental data of the PRF at three temperatures are shown in Table 2 for the model constants and Table 3 for the statistical indicators. The best model was selected based on: $P_e \leq 10$, $R^2 > 0.95$, low SSE and low RMSE for

Table 2: Means and (standard deviations) of the empirical parameters of the proposed mathematical models for simulating the experimental sorption isotherm curves of PRF at different temperatures.

P*	Adsorption			Desorption		
	25 °C	35 °C	45 °C	25 °C	35 °C	45 °C
Peleg model (MN 1) $X_e = C_1(a_w)^{C_2} + C_3(a_w)^{C_4}$						
C1	0.180	0.169	0.194	0.176	−0.054	0.216
	(0.025)$^+$	(0.007)	(0.017)	(0.548)	(0.344)	(0.630)
C2	3.38	3.119	4.180	0.981	1.274	0.692
	(3.06)	(2.756)	(3.639)	(0.123)	(0.717)	(0.463)
C3	0.189	0.163	0.203	0.074	0.305	0.049
	(0.019)	(0.008)	(0.018)	(0.551)	(0.340)	(0.621)
C4	5.29	4.714	6.292	0.851	0.558	1.136
	(3.21)	(2.77)	(3.651)	(0.289)	(1.619)	(0.222)
GAB model (MN 2) $X_e = \frac{X_m CKa_w}{(1-Ka_w)(1-Ka_w+CKa_w)}$						
X_m	0.109	0.149	0.860	6.447	1.045	3.274
	(0.006)	(0.010)	(0.278)	(2.198)	(0.539)	(2.22)
C	0.666	0.632	0.067	0.134	0.575	0.145
	(0.029)	(0.047)	(0.021)	(0.064)	(0.208)	(0.093)
K	0.790	0.719	0.710	0.223	0.312	0.380
	(0.004)	(0.007)	(0.013)	(0.010)	(0.031)	(0.057)
BET model (MN 3) $X_e = \frac{X_m ca_w}{[(1-a_w)+(c-1)(1-a_w)a_w]}$						
X_m	0.036	0.041	0.032	0.046	0.044	0.039
	(0.0002)	(0.000)	(0.004)	(0.000)	(0.004)	(0.007)
C	2.313	2.433	2.309	2427.6	−1860.04	17.39
	(0.032)	(0.016)	(0.924)	(204.97)	(1621.35)	(11.25)
Halsey model (MN 4) $X_e = \left(-\frac{A}{\ln a_w}\right)^{1/B}$						
A	0.022	0.021	0.027	0.0097	0.010	0.0145
	(0.0003)	(0.0001)	(0.002)	(0.002)	(0.0002)	(0.0008)
B	1.173	1.231	1.052	1.848	1.786	1.571
	(0.002)	(0.001)	(0.011)	(0.079)	(0.015)	(0.009)
Oswin model (MN 5) $X_e = k(a_w/1-a_w)^n$						
K	0.054	0.060	0.046	0.103	0.09	0.0718
	(0.0006)	(0.0001)	(0.002)	(0.0008)	(0.0007)	(0.022)
N	0.699	0.660	0.794	0.438	0.445	0.667
	(0.0007)	(0.0004)	(0.002)	(0.016)	(0.004)	(0.142)
Smith model (MN 6) $X_e = A - B(\ln(1-a_w))$						
A	−0.0134	−0.0118	−0.022	0.014	0.019	−0.005
	(0.000)	(0.002)	(0.001)	(0.0003)	(0.007)	(0.003)
B	0.102	0.104	0.106	0.126	0.111	0.131
	(0.0009)	(0.002)	(0.005)	(0.0003)	(0.012)	(0.001)
Modified Henderson model (MN 7) $X_e = \{\ln(1-a_w)/[-k(T+c)]\}^{1/n}$						
K	0.276	0.232	0.137	0.417	0.399	0.364
	(0.022)	(0.0006)	(0.004)	(0.026)	(0.075)	(0.183)
C	1.10	0.768	0.369	0.239	0.475	0.404
	(0.981)	(0.202)	(0.196)	(0.287)	(0.276)	(0.357)
n	0.808	0.892	0.706	1.209	1.319	1.023
	(0.014)	(0.002)	(0.002)	(0.025)	(0.093)	(0.127)
Adam and Shove model (MN 8) $X_e = A + Ba_w + Ca_w{}^2 + Da_w{}^3$						
A	−0.022	−0.029	−0.019	0.0043	0.002	−0.004
	(0.0005)	(0.007)	(0.0008)	(0.0006)	(0.001)	(0.0006)
B	0.265	0.355	0.219	0.085	0.107	0.034
	(0.006)	(0.096)	(0.008)	(0.005)	(0.009)	(0.002)
C	−0.532	−0.755	−0.512	0.379	0.263	0.435
	(0.014)	(0.302)	(0.022)	(0.013)	(0.09)	(0.031)
D	0.594	0.756	0.636	−0.241	−0.124	−0.212
	(0.011)	(0.232)	(0.028)	(0.011)	(0.024)	(0.019)

(*continued*)

Table 2: (*continued*)

P*	Adsorption			Desorption		
	25 °C	35 °C	45 °C	25 °C	35 °C	45 °C
Modified Oswin model (MN 9) $X = (A + BT)\left[\frac{a_w}{(1-a_w)}\right]^C$						
A	0.388	0.715	0.295	0.363	0.244	0.352
	(0.375)	(0.441)	(0.212)	(0.097)	(0.203)	(0.296)
B	−0.0134	−0.019	−0.006	−0.01	−0.004	−0.006
	(0.015)	(0.012)	(0.005)	(0.003)	(0.006)	(0.006)
C	0.699	0.723	0.794	0.574	0.528	0.542
	(0.0007)	(0.076)	(0.002)	(0.105)	(0.004)	(0.051)
Modified Halsey model (MN 10) $X = \left[-\frac{\exp(A+BT)}{\ln a_w}\right]^C$						
A	28.99	−434.38	−108.4	2.05	−71.34	−81.52
	(51.69)	(504.44)	(120.45)	(2.18)	(102.03)	(65.32)
B	−1.294	12.3	2.328	−0.263	1.925	1.718
	(2.063)	(14.41)	(2.676)	(0.083)	(2.92)	(1.45)
C	0.942	0.806	0.955	0.555	0.663	0.639
	(0.118)	(0.010)	(0.002)	(0.025)	(0.105)	(0.002)

Note: *P = empirical parameters. [+]Numbers in parentheses represent standard deviations.

Table 3: Values of the statistical indicators (SI) of the proposed mathematical models for simulating the experimental sorption isotherm curves of FRP at different temperatures.

		Adsorption			Desorption		
MN*	**SI**	**25 °C**	**35 °C**	**45 °C**	**25 °C**	**35 °C**	**45 °C**
1	SSE	2.92×10^{-5}	5.77×10^{-5}	2.30×10^{-5}	2.68×10^{-4}	2.62×10^{-4}	3.76×10^{-4}
	R^2	0.999	0.998	0.999	0.993	0.993	0.990
	RMSE	0.002	0.003	0.002	0.007	0.007	0.009
	P_e	4	3	10	4	6	10
2	SSE	5.85×10^{-5}	9.65×10^{-5}	7.84×10^{-5}	4.86×10^{-5}	3.43×10^{-4}	9.39×10^{-4}
	R^2	0.998	0.997	0.998	0.987	0.991	0.980
	RMSE	0.003	0.004	0.004	0.009	0.008	0.012
	P_e	7	5	23	7	6	101
3	SSE	5.94×10^{-4}	7.64×10^{-4}	7.51×10^{-4}	8.45×10^{-3}	1.43×10^{-2}	9.35×10^{-3}
	R^2	0.983	0.979	0.981	0.775	0.637	0.805
	RMSE	0.009	0.010	0.010	0.035	0.044	0.036
	P_e	13	12	43	18	17	23
4	SSE	1.15×10^{-3}	1.56×10^{-3}	1.19×10^{-3}	4.97×10^{-3}	4.55×10^{-3}	6.14×10^{-3}
	R^2	0.967	0.957	0.969	0.868	0.885	0.869
	RMSE	0.013	0.015	0.013	0.027	0.025	0.030
	P_e	27	24	68	44	44	313
5	SSE	4.52×10^{-4}	6.97×10^{-4}	5.11×10^{-4}	2.89×10^{-3}	2.72×10^{-3}	2.16×10^{-3}
	R^2	0.987	0.981	0.987	0.923	0.931	0.952
	RMSE	0.008	0.010	0.009	0.020	0.020	0.017
	P_e	17	16	47	31	32	160
6	SSE	1.04×10^{-4}	7.45×10^{-4}	4.63×10^{-4}	1.51×10^{-3}	1.78×10^{-3}	7.63×10^{-4}
	R^2	0.997	0.980	0.988	0.960	0.955	0.984
	RMSE	0.004	0.009	0.008	0.015	0.016	0.010
	P_e	9	7	19	17	64	68
7	SSE	4.27×10^{-5}	1.11×10^{-4}	5.78×10^{-5}	7.95×10^{-4}	8.78×10^{-4}	1.35×10^{-3}
	R^2	0.999	0.997	0.999	0.979	0.978	0.972
	RMSE	0.003	0.004	0.003	0.012	0.012	0.015

(*continued*)

Table 3: (*continued*)

		Adsorption			Desorption		
MN*	**SI**	**25 °C**	**35 °C**	**45 °C**	**25 °C**	**35 °C**	**45 °C**
	P_e	6	5	19	11	15	86
8	SSE	3.38×10^{-5}	4.22×10^{-4}	9.31×10^{-5}	2.05×10^{-4}	2.24×10^{-4}	3.44×10^{-4}
	R^2	0.999	0.988	0.998	0.995	0.994	0.993
	RMSE	0.003	0.008	0.004	0.006	0.007	0.008
	P_e	7	9	19	6	6	22
9	SSE	4.52×10^{-4}	1.05×10^{-3}	5.11×10^{-4}	2.11×10^{-3}	1.36×10^{-3}	3.38×10^{-3}
	R^2	0.987	0.971	0.987	0.944	0.966	0.929
	RMSE	0.009	0.013	0.009	0.018	0.015	0.023
	P_e	17	17	51	23	24	220
10	SSE	2.58×10^{-2}	1.60×10^{-3}	1.16×10^{-3}	4.76×10^{-3}	5.44×10^{-3}	6.64×10^{-3}
	R^2	0.270	0.956	0.970	0.873	0.862	0.860
	RMSE	0.056	0.016	0.014	0.028	0.030	0.033
	P_e	50	64	62	43	47	212

Note: *MN, model number (see Table 1).

all temperatures. By applying that, it can be noticed that the Peleg model was the best model to describe the experimental adsorption and desorption isotherms of PRF over a wide range of water activity (0.09–0.87). Comparing to the other models, the Peleg model was the highest in R^2, and the lowest in SSE, RMSE, and P_e values. The ranges of R^2, SSE, RMSE and P_e are 0.990–0.999, 2.30×10^{-5}–2.76×10^{-4}, 0.002–0.009 and 3–10 for both adsorption and desorption isotherms of the PRF, respectively. The observed and predicted sorption isotherms using the Peleg model are jointly shown with the real data points in Figures 2 and 3. Therefore, Peleg model can be recommended with the corresponding parameters for the prediction of the adsorption and desorption isotherms of PRF at the different temperatures (25, 35 and 45 °C) and water activity ranging from 0.09 to 0.87.

Also, Figures 4–6 show the experimental data of adsorption and desorption isotherms of PRF as fitted by the Peleg model, where a good agreement between experimental and predicted data can be observed. Peleg model was successfully applied to several agricultural products such as starch powders [3], orange peel and leaves [17] and Tunisian olive leaves [18]. Further, this model provides a good representation of Type II (sigmoidal) and III (non-sigmoidal) sorption isotherms [51] and it is also useful for validating a new proposed model applied to different products [57].

The adsorption isotherms are essential to select the appropriate storage conditions. Consequently, the equilibrium values of moisture content of PRF at the microbial safe water activity of 0.6 [58] and a selected temperature were experimentally determined. The PRF should be stored at a maximum moisture content of 7.1, 8.5 and 6.1 d.b. (%) in order to prevent the growth of microorganisms or quality deterioration at temperatures 25, 35 and 45 °C respectively. Larrauri [38] recommended a value of 9 d.b. (%) or less for fibers.

3.5 Isosteric heat of sorption and the differential entropy

Knowledge of the differential heat of sorption is important when designing equipment for dehydration processes. This is due to the fact that the heat of vaporization of sorbed water may increase to values above the heat of vaporization of pure water as food is dehydrated to low moisture levels [54].

The isosteric heat of sorption as affected by different moisture content of PRF is shown in Figure 7, where the isosteric heat increased by decreasing the moisture content. It has been reported that the high values of isosteric heat at low moisture contents are explained by tight bonds of water molecules to the food constituting a monolayer of molecules. Therefore the amount of energy required to remove these water molecules is high. The values of Q_{st} are higher than λ, indicating that the energy of binding between the water molecules and the sorption sites is higher than the energy which holds the molecules of pure water together in the liquid phase [59]. The increase in the isosteric heat with decreasing moisture content of the PRF agrees with the results of other studies for several products such as Tunisian olive leaves [18],

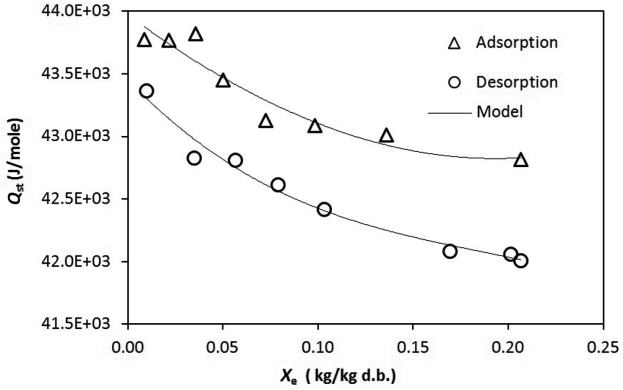

Figure 7: Experimental and predicted values of isosteric heat of adsorption and desorption for PRF as a function of equilibrium moisture content.

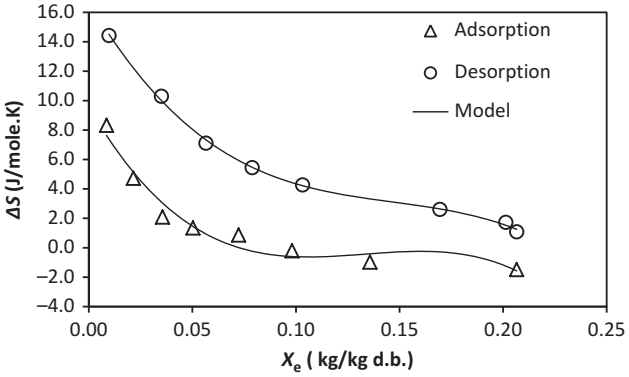

Figure 8: Experimental and predicted values of differential entropy of adsorption and desorption for PRF as a function of equilibrium moisture content.

grapes, apricots, apples and potatoes [19], sultana raisins, figs, prunes and apricots [23], starch powders [26], black and green tea [28] and potatoes [53].

The Q_{st} versus X_e results can be adequately represented by polynomial eqs (4) and (5) for the adsorption and desorption, respectively.

$$(Q_{st})_{Ad} = 15.808X_e^3 + 24.736X_e^2 - 11.322X_e + 43.97;\ R^2 = 0.915 \quad (4)$$

$$(Q_{st})_{De} = -120.62X_e^3 + 68.078X_e^2 - 15.888X_e + 43.455;\ R^2 = 0.978 \quad (5)$$

The differential entropy of adsorption and desorption, at each moisture content, was calculated by applying eq. (1) to the experimental data. The differential entropy was plotted as a function of moisture content as shown in Figure 8 for both adsorption and desorption. It was found that the entropy data display a strong dependence on moisture content. The differential entropy of desorption exhibits higher values than that for adsorption. It indicates that water molecules are more mobile during desorption than adsorption [26]. The result is similar to that reported by other researchers [26, 27].

The differential entropy versus moisture content results can be predicted by polynomial functions as shown in eqs (6) and (7) for the adsorption and desorption, respectively.

$$(\Delta S)_{Ad} = -3412.9X_e^3 + 1504.7X_e^2 - 240.04X_e + 16.714;\ R^2 = 0.999 \quad (6)$$

$$(\Delta S)_{De} = -4854.5X_e^3 + 1939.6X_e^2 - 247.66X_e + 9.6133;\ R^2 = 0.963 \quad (7)$$

3.6 Water plasticization behavior

Values of T_g obtained for the different samples as a function of moisture content are shown in Figure 9. The water plasticization effect can be observed, where increasing the water content resulted in a decrease in the glass transition temperatures. This observation is similar to that obtained for several food products such as spray dried tomato pulp powder [33], freeze-dried pineapple powder [34], freeze-dried onion powder [35], Kiwi fruit [36] and papaya [37].

It can be noticed also in Figure 9 that the real data can be predicted successfully by Gordon and Taylor model (eq. (4)). The Gordon and Taylor model can be considered a reliable predictor of glass transition temperatures of PRF at different moisture contents. It was fitted to experimental points using $T_{gw} = -135$ °C, with the following parameters calculated by non-linear

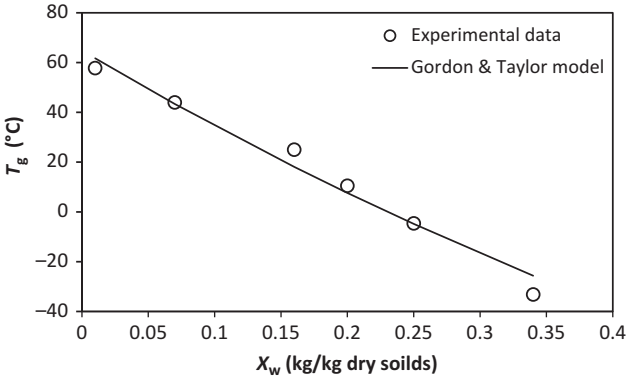

Figure 9: Relationship between glass transition temperature (T_g) and moisture content (X_w) of PRF.

regression: $T_{gs} = 64.92\,°C$ and k = 1.607, where $R^2 = 0.976$. From Figure 9, it can be recommended that the PRF with $X_w \leq 9\,\%$ should be stored at temperature less than 35 °C to avoid formulation to a rubbery state which can cause agglomeration and stickiness.

4 Conclusion

The moisture sorption curves of PRF obtained at three temperatures (25, 35, and 45 °C (and a wide range of water activity (0.09–0.87) showed type III shape. The moisture adsorption increased as the relative humidity increased while in the case of the desorption process, the equilibrium moisture content decreased with the decreasing relative humidity. It took up to 29 and 25 h to reach the equilibrium state for the adsorption and desorption process respectively. The hysteresis phenomenon was observed. The best fitted model representing equilibrium moisture data for both adsorption and desorption was the Peleg model. The isosteric heats of sorption and the differential entropy of PRF decreased as the moisture content increased and can be predicted by polynomial functions. Water can be considered a plasticizer in PRF where the glass transition temperature decreased by increasing the moisture content (X_w). Gordon and Taylor model represented adequately the relationship between glass transition temperature and moisture content. The PRF should be stored at minimum moisture content of 9 d.b. (%) and temperature less than 35 °C.

Acknowledgment: The authors acknowledge the financial support of the center of researches, College of food and agricultural sciences, Deanship of scientific research, King Saud University and appreciate the technical support of King Abdullah institute for nanotechnology.

References

1. Fikry M. Production and characterization of powders rich in fiber from Palm Date flesh and seed. Riyadh, KSA: King Saud University (Thesis), 2016.
2. Foster KD, Bronlund JE. The prediction of moisture sorption isotherms for dairy powders. Int Dairy J 2005;15:411–18.
3. Al-Muhtaseb AH, McMinn WA, Magee TR. Water sorption isotherms of starch powders. J Food Eng 2004;61:297–307.
4. Basu S, Shivhare US, Mujjumdar AS. Models for sorption Isotherms for foods: a review. Drying Technol 2006;24:917–30.
5. Bingol G, Prakash B, Pan Z. Dynamic vapor sorption isotherms of medium grain rice varieties. LWT – Food Sci Technol 2012;48:156–63.
6. Rahman MS, Al-Belushi RH. Dynamic isopiestic method (DIM): measuring moisture sorption isotherm of freeze-dried garlic powder and other potential uses of DIM. Int J Food Prop 2006;9:421–37.
7. Roman-Gutierrez AD, Guilbert S, Cuq B. Distribution of water between wheat flour components: a dynamic water vapor adsorption study. J Cereal Sci 2002;36:347–55.
8. Young PM, Edge S, Staniforth JN, Steele DF, Price R. Dynamic vapor sorption properties of sodium starch glycolate disintegrants. Pharm Dev Technol 2005;10:249–59.
9. Arlabosse P, Rodier E, Ferrasse JH, Chavez S, Lecomate D. Comparison between static and dynamic methods for sorption isotherm measurements. Drying Technol 2003;21:479–97.
10. Gomez GI, Orrego-alzate CE, Grajales LM, Telis VR, Gabas AL, Telis-Romero J. Effect of drying methods on the thermodynamic properties of Blackberry pulp powder. Dyna 2011;78:139–48.
11. Falade KO, Aworh OC. Adsorption isotherms of osmo-oven dried African star apple (*Chrysophyllum albidum*) and African mango (*Irvingia gabonensis*) slices. Eur Food Res Technol 2004;218:278–83.
12. Falade KO, Adetunji AI, Aworh OC. Adsorption isotherm and heat of sorption of fresh- and osmo-oven dried plantain slices. Eur Food Res Technol 2003;217:230–4.
13. Khalloufi S, El-Maslouhi Y, Ratti C. Mathematical model for prediction of glass transition temperature of fruit powders. J Food Sci 2000;65:842–8.
14. Falade KO, Olukini I, Adegoke GO. Adsorption isotherm and heat of sorption of osmotically pretreated and air-dried pineapple slices. Eur Food Res Technol 2004;218:540–3.
15. Argyropoulos D, Alex R, Kohler R, Müller J. Moisture sorption isotherms and isosteric heat of sorption of leaves and stems of lemon balm (*Melissa officinalis* L.) established by dynamic vapor sorption. LWT – Food Sci Technol 2012;47:324–31.
16. Viganó J, Azuara E, Telis VR, Beristain CI, Jiménez M, Telis-Romero J. Role of enthalpy and entropy in moisture sorption behavior of pineapple pulp powder produced by different drying methods. Thermochim Acta 2012;528:63–71.
17. Kammoun Bejar A, Boudhrioua Mihoubi N, Kechaou N. Moisture sorption isotherms – experimental and mathematical investigations of orange (*Citrus sinensis*) peel and leaves. Food Chem 2012;132:1728–35.
18. Bahloul N, Boudhrioua N, Kechaou N. Moisture desorption–adsorption isotherms and isosteric heats of sorption of Tunisian olive leaves (*Olea europaea* L.). Ind Crops Prod 2008;28:162–76.
19. Kaymak-Ertekin F, Gedik A. Sorption isotherms and isosteric heat of sorption for grapes, apricots, apples and potatoes. LWT – Food Sci Technol 2004;37:429–38.
20. Garcı´a-Pe´rez JV, Cárcel JA, Clemente G, Mulet A. Water sorption isotherms for lemon peel at different temperatures and isosteric heats. LWT – Food Sci Technol 2008;41:18–25.
21. Jamali A, Kouhila M, Mohamed LA, Idlimam A, Lamharrar A. Moisture adsorption-desorption isotherms of *Citrus reticulata* leaves at three temperatures. J Food Eng 2006;77:71–8.
22. Silva VM, Viotto LA. Drying of sicilian lemon residue influence of process variables on the evaluation of the dietary fiber produced. Ciênc Tecnol Aliment Campinas 2010;2:421–8.
23. Tsami E, Maroulis ZB, Morunos-Kouris D, Saravacos GD. Heat of sorption of water in dried fruits. Int J Food Sci Technol 1990;25:350–9.

24. Rizvi SSH. Thermodynamic properties of food in dehydration. In: Rao MA, Datta AK, Rizvi SSH, editors. Engineering properties of foods. New York: Marcel Dekker Inc., 1995:223–309.
25. Wang N, Brennan JG. Moisture sorption isotherm characteristics of potatoes at four temperatures. J Food Eng 1991;14:269–82.
26. Al-Muhtaseb AH, McMinn WA, Magee TR. Water sorption isotherms of starch powders. Part 2: Thermodynamic characteristics. J Food Eng 2004;62:135–42.
27. Kane CS, Kouhila M, Lamharrar A, Idlimam A, Mimet A. Moisture sorption isotherms and thermodynamic properties of tow mints: *Mentha pulegium* and *Mentha rotundifolia*. Rev Energies Renouvelables 2008;11:181–95.
28. Ghodake HM, Goswami TK, Chakraverty A. Moisture sorption isotherms, heat of sorption and vaporization of withered leaves, black and green tea. J Food Eng 2007;78:827–35.
29. Jamali A, Kouhila M, Ait Mohamed L, Jaouhari JT, Idlimam A, Abdenouri N. Sorption isotherms of *Chenopodium ambrosioides* leaves at three temperatures. J Food Eng 2006;72:77–84.
30. Madamba PS, Driscoll RH, Buckle KA. Enthalpyentropy compensation models for sorption and browning of garlic. J Food Eng 1996;28:109–19.
31. Ross YH. Glass transition – related physicochemical changes in foods. Food Technol 1995;45:97–102.
32. Roos YH, Karel M. Applying state diagrams to food processing and development. Food Technol 1991;45:66–71.
33. Goula AM, Karapantsios TD, Achilias DS, Adamopoulos KG. Water sorption isotherms and glass transition temperature of spray dried tomato pulp. J Food Eng 2008;85:73–83.
34. Telis VRN, Sobral PJA, Transitions G. State diagram for freeze-dried pineapple. LWT – Food Sci Technol 2001;34:199–205.
35. Sá MM, Sereno AM. Glass transitions and state diagrams for typical natural fruits and vegetables. Thermochim Acta 1994;246:285–97.
36. Moraga G, Martínez-Navarrete N, Chiralt A. Water sorption isotherms and phase transitions in kiwifruit. J Food Eng 2006;72:147–56.
37. Kurozawa LE, Hubinger MD, Park KJ. Glass transition phenomenon on shrinkage of papaya during convective drying. J Food Eng 2012;108:43–50.
38. Larrauri JA. New approaches in the preparation of high dietary fibre powders from fruit by-products. Trends Food Sci Technol 1999;10:3–8.
39. MATLAB. MathWorks, Inc. Software program, version R2010a. 2010.
40. Peleg M. Assessment of a semi-empirical four parameter general model for sigmoid moisture sorption isotherms. J Food Process Eng 1993;16:21–37.
41. Van den Berg C. Water activity and its estimation in food systems: theoretical aspects. In: Rockland LB, Stewart GE, editors. Water Activity: Influences on Food Quality. New York: Academic Press. 1981:1–61.
42. Brunauer S, Emmett PH, Teller E. Adsorption of gases in multimolecular layers. J Am Chem Soc 1938;60:309–20.
43. Halsey G. Physical adsorption on non-uniform surfaces. J Chem Phys 1948;16:931–7.
44. Oswin CR. The kinetics of package life III. The isotherm. J Soc Chem Ind 1946;65:419–21.
45. Smith SE. The sorption of water vapor by high polymers. J Am Chem Soc 1947;69:646.
46. Henderson SM. A basic concept of equilibrium moisture. Agric Eng 1952;33:29–32.
47. Chirife J, Iglesias HA. Equations for fitting water sorption isotherms of foods. Part I. A review. J Food Technol 1978;13:159–74.
48. Chen CS. Equilibrium moisture curves for biological materials. Trans ASEA 1971;14:924–6.
49. Iglesias HA, Chirife J. Prediction of the effect of temperature on water sorption isotherms of food material. J Food Technol 1976;11:109–16.
50. Gordon M, Taylor JS. Ideal copolymers and the second order transitions of synthetic rubbers. I. Non-crystalline copolymers. J Appl Chem 1952;2:493–500.
51. Brunauer S. The adsorption of gases and vapors. Physical adsorption. Princeton, NJ: Princeton University Press, 1945.
52. Kaya S, Kahyaoglu T. Moisture sorption and thermodynamic properties of safflower petals and tarragon. J Food Eng 2007;78:413–21.
53. McLaughlin CP, Magee TR. The determination of sorption isotherm and the isosteric heats of sorption for potatoes. J Food Eng 1998;53:267–80.
54. Al-Muhtaseb AH, McMinn WA, Magee TRA. Moisture sorption isotherm characteristics of food products: a review. Food Bioprod Process 2002;80:118–28.
55. Al Hodali R. Numerical simulation of an agricultural foodstuffs drying unit using solar energy and adsorption process. Belgium: Universite´ Libre de Bruxelles, 1997.
56. Moreira R, Chenlo F, Vázquez MJ, Cameán P. Sorption isotherms of turnip top leaves and stems in the temperature range from 298 to 328 K. J Food Eng 2005;71:193–9.
57. Lewicki PP. A three parameter equation for food moisture sorption isotherms. J Food Process Eng 1998;21:127–44.
58. Cordeiro DS, Raghavan GS, Oliveira WP. Equilibrium moisture content models for *Maytenus ilicifolia* leaves. Biosyst Eng 2006;94:221–8.
59. Masuzawa M, Sterling C. Gel water relationships in hydrophilic polymers: thermodynamics of sorption of water vapor. J Appl Polym Sci 1968;12:2023–32.